Proceedings of the ASME 2013 Pressure Vessels and Piping Conference
PVP2013
July 14-18, 2013, Paris, France

PVP2013-97016

FURTHER INSIGHTS ON *J-R* CURVE BEHAVIOR IN PIPELINE STEELS USING LOW CONSTRAINT FRACTURE SPECIMENS

Diego F. B. Sarzosa
Dept. of Naval Architecture and Ocean Engineering, University of São Paulo
São Paulo, SP 05508-900, Brazil
dsarzosa@usp.br

Claudio Ruggieri
Dept. of Naval Architecture and Ocean Engineering, University of São Paulo
São Paulo, SP 05508-900, Brazil
claudio.ruggieri@poli.usp.br

ABSTRACT

This work addresses a two-parameter description of crack-tip fields in bend and tensile fracture specimens incorporating the evolution of near-tip stresses following stable crack growth with increased values of the J-integral. The primary objective is to examine the potential coupled effects of geometry and ductile tearing on crack-tip constraint as characterized by the J-Q theory which enables more accurate correlations of crack growth resistance behavior in conventional fracture specimens. Plane-strain, finite element computations including stationary and growth analyses are described for SE(B) and clamped SE(T) specimens having different notch depth to specimen width ratio in the range $0.2 \leq a/W \leq 0.5$. A computational cell methodology to model Mode I crack extension in ductile materials is utilized to describe the evolution of J with Δa for the fracture specimens. Laboratory testing of an API 5L X70 steel using deeply cracked C(T) specimens is used to measure the crack growth resistance curve for the material and to calibrate the cell parameters. The present results provide additional understanding of the effects of constraint on crack growth which contributes to further evaluation of crack growth resistance properties of pipeline steels using SE (T) and SE(B) specimens.

INTRODUCTION

Standardized techniques for crack growth resistance testing of structural steels, including ASTM 1820 [1] and ISO 15653 [2], routinely employ three-point bend SE(B) and compact tension C(T) specimens containing deep, through cracks ($a/W \geq 0.45 \sim 0.5$). The primary motivation to use deeply cracked specimens is to guarantee conditions leading to crack growth under high crack-tip constraint with limited-scale plasticity [3,4]. Under such conditions, a single crack growth resistance curve in terms of J-Δa data characterizes the increase in fracture toughness over the first few mm of stable crack extension; here, the J-integral describes the intensity of near-tip deformation [3,4] and Δa is the amount of crack growth. However, a variety of crack-like defects are most often surface cracks formed during in-service operation and exposure to aggressive environment or during welding fabrication [5]. Structural components falling into this category include girth welds made in field conditions for high pressure piping systems and steel catenary risers. These crack configurations generally develop low levels of crack-tip stress triaxiality which contrast sharply to conditions present in deeply cracked specimens [6].

Recent defect assessment procedures [7] advocate the use of single edge notch tension (SE(T)) specimens under clamp conditions to characterize the fracture properties of girth welds in deep water steel catenary risers installed by the pipe reeling process. Here, the welded pipe is coiled around a large diameter reel on a vessel and then unreeled, straightened and finally deployed to the sea floor after subjecting the pipe to high levels of bending load and plastic deformation with potential strong impact on unstable crack propagation of undetected (circumferential) flaws at girth welds. The primary motivation to use clamped SE(T) fracture specimens in defect assessment procedures of pipeline girth welds under bending is the strong similarity in crack-tip stress and strain fields which drive the fracture process for both crack configurations [8]. Recent applications of SE(T) fracture specimens to characterize crack growth resistance properties in pipeline steels [9] have been effective in providing larger flaw tolerances while, at the same time, reducing the otherwise excessive conservatism which arises when measuring the material's fracture toughness based on high constraint, deeply-cracked, single edge notch bend (SE(B)) or compact tension (C(T)) specimens.

However, while now utilized effectively in fracture testing of pipeline girth welds, some difficulties associated with SE(T) testing procedures, including fixture and gripping conditions, raise concerns about the significance and qualification of measured crack growth resistance curves. Such uncertainties in measured fracture toughness may potentially affect tolerable defect sizes obtained from ECA procedures. While slightly more conservative, testing of shallow-crack bend specimens may become more attractive due to its simpler testing protocol, laboratory procedures and much smaller loads required to propagate the crack. Although, deeply-cracked SE(B) specimens are the preferred crack geometry often adopted in conventional defect assessment methods, recent revisions of ASTM 1820 [1] and ISO 15653 [2] have included J-estimation equations applicable to shallow-crack bend specimens. Consequently, use of smaller specimens which yet guarantee adequate levels of crack-tip constraint to measure the material's fracture toughness emerges as a highly effective alternative.

Motivated by these observations, this investigation addresses a two-parameter description of crack-tip fields in bend and tensile fracture specimens incorporating the evolution of near-tip stresses following stable crack growth with increased values of the crack driving force as characterized by J. The primary objective is to examine the potential coupled effects of geometry and ductile tearing on crack-tip constraint as characterized by the J-Q theory which enables more accurate correlations of crack growth resistance behavior in conventional fracture specimens. Plane-strain, finite element computations including stationary and growth analyses are conducted for 3P SE(B) and clamped SE(T) specimens having different notch depth to specimen width ratio in the range $0.2 \leq a/W \leq 0.5$. For the growth analyses, the models are loaded to levels of J consistent to a crack growth resistance curve, J-Δa, representative of a typical pipeline steel. A computational cell methodology to model Mode I crack extension in ductile materials is utilized to describe the evolution of J with Δa and the accompanying evolving near-tip opening stresses. Laboratory testing of an API 5L X70 steel at room temperature using standard, deeply cracked C(T) specimens is used to measure the crack growth resistance curve for the material and to calibrate the key cell parameter defined by the initial void fraction, f_0. The present results provide additional understanding of the effects of constraint on crack growth which contributes to further evaluation of crack growth resistance properties of pipeline steels using SE (T) and SE(B) specimens while, at the same time, eliminating some restrictions against the use of shallow cracked bend specimens in defect assessment procedures.

OVERVIEW OF THE COMPUTATIONAL CELL MODEL FOR DUCTILE TEARING

This section presents a summary of the cell-based framework to model stable crack growth in ductile materials. Further details of the cell model are found in [10-12]. Ductile fracture in metals is a process of material failure which incorporates various and simultaneous mechanisms at the microscale level [13]. The commonly observed stages of this process are: a) formation of a free surface at an inclusion or second phase particle by either decohesion or particle cracking; b) growth of a void around the particle by means of plastic strain and hydrostatic stress; and c) coalescence of the growing void with adjacent voids. Experimental observations and computational studies show that the plastic strains for nucleation are small thereby causing only little damage in the material ahead of the crack tip. This feature enables simplification of the ductile failure process by assuming the growth of microvoids as the critical event controlling ductile extension. Figure 1(a) pictures the schematic path of a growing crack in a ductile material. The material layer enveloping the growing crack, which must be thick enough to include at least a void or microcrack nuclei, identifies a process zone for the ductile fracture which conveniently gives the necessary length dimension for the model. Void growth and coalescence in the layer will cause

material softening ahead of crack tip thereby reducing its macroscopic stress capacity. Computational approaches to model such progressive damage of material ahead of the extending crack have developed along essentially two lines of investigation: (1) cohesive-law fracture models defined on the crack plane and a specific strength for the material (peak stress ahead of the crack) coupled with an explicit length-scale over which damage occurs, and (2) continuum damage plasticity models that predict the softening of material in a continuum context due to the idealized growth of a spherical void or a periodic array of voids.

Motivated by the above observations, Xia and Shih [10] proposed a model using *computational cells* to include a realistic void growth mechanism and a microstructural length-scale physically coupled to the size of the fracture process zone. Void growth remains confined to a layer of material symmetrically located about the crack plane, as illustrated in Fig. 1(b), and having thickness D, where D is associated with the mean spacing of the larger, void initiating inclusions. This layer consists of cubical cell elements with dimension D on each side; each cell contains a cavity of initial volume fraction f_0 (the initial void volume divided by cell volume). As a further simplification, the void nucleates from an inclusion of relative size f_0 immediately upon loading. Progressive void growth and subsequent macroscopic material softening in each cell are described with the Gurson-Tvergaard (GT) constitutive model for dilatant plasticity [14,15] given by

$$\left(\frac{\sigma_e}{\overline{\sigma}}\right)^2 + 2q_1 f \cosh\left(\frac{3q_2\sigma_m}{2\overline{\sigma}}\right) - (1 + q_3 f^2) = 0 \qquad (1)$$

where σ_e denotes the effective Mises (macroscopic) stress, σ_m is the mean (macroscopic) stress, $\overline{\sigma}$ is the current flow stress of the cell matrix material and f defines the current void fraction. Factors q_1, q_2 and q_3 introduced by Tvergaard [15] improve the model predictions for periodic arrays of cylindrical and spherical voids. The present analyses use $q_1 = 1.43$, $q_2 = 0.97$ and $q_3 = q_1^2$. These q-values are obtained from the work of Faleskog [16] which provides the micromechanics parameters q_1 and q_2 for a wide range of material flow properties (strain hardening properties and yield stress) for common pressure vessel and structural steels. Using an experimental J-Δa curve obtained from a conventional, deeply cracked SE(B) or C(T) specimen, a series of finite element analyses of the specimen are conducted to *calibrate* values for the cell parameters D and f_0 which bring the predicted J-Δa curve into agreement with experiments as described later in the article.

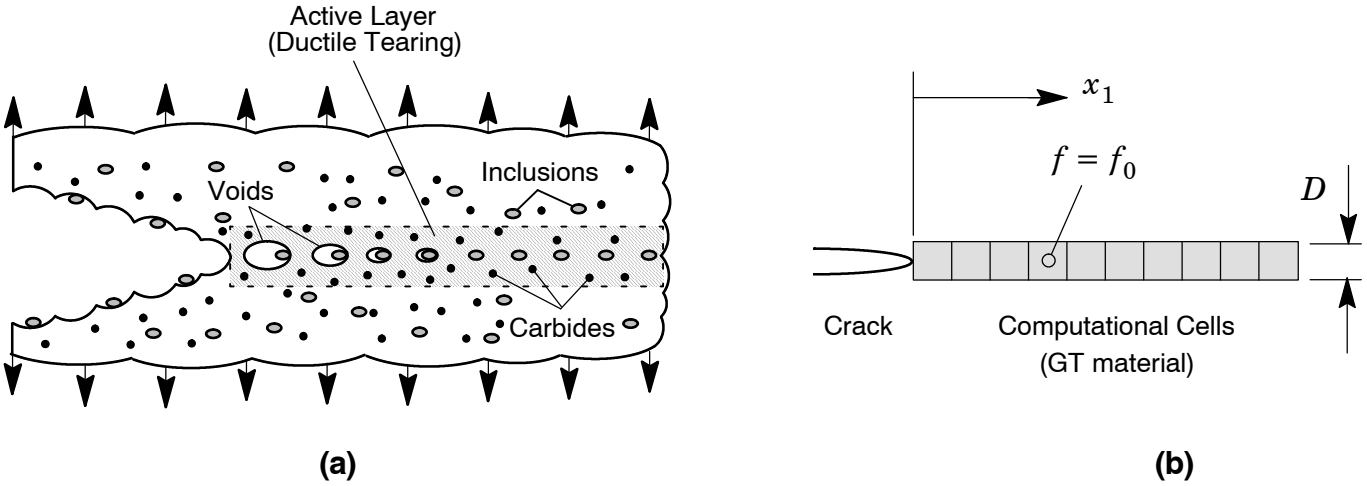

Figure 1. Modeling of ductile tearing using computational cells.

Further improvement in the cell methodology introduced by Ruggieri and Dodds (R&D) [11] enables the model to create new traction free surfaces to represent physical crack extension. When f in the cell incident on the current crack tip reaches a critical value, f_E, the computational procedures remove the cell thereby advancing the crack tip in discrete increments of the cell size (Tvergaard [15] refers to this process as the element extinction or vanish technique). R&D [11] implements a cell extinction process using a linear-traction separation model with f_E typically assigned a value of $\approx 0.15 \sim 0.20$. The final stage of void linkup

with the macroscopic crack front then occurs by reducing the remaining stresses to zero in a prescribed linear manner.

THE *J-Q* APPROACH

Constraint in Stationary Cracks: The Q-Parameter

Much research in the the last 10∼20 years has convincingly demonstrated the strong effects of specimen geometry and loading mode (bending *vs.* tension) on fracture behavior for ferritic structural steels in the ductile-to-brittle (DBT) transition region as well as in the upper shelf region. At increased loads in a finite body, such as a cracked specimen or structure, the initially strong small scale yielding (SSY) fields gradually change to fields under large scale yielding (LSY) as crack-tip plastic zones increasingly merge with the global bending plasticity on the nearby traction free boundaries. This phenomenon, often termed *loss of constraint*, contributes to the *apparent* increased toughness of shallow cracked and tension loaded geometries observed in fracture testing [17-20].

The above arguments motivated O'Dowd and Shih (OS) [21,22] to propose an approximate two-parameter description for the elastic-plastic crack tip fields based upon a triaxiality parameter more applicable under large scale yielding (LSY) conditions for materials with elastic-plastic response described by a power hardening law given by $\epsilon/\epsilon_0 \propto (\sigma/\sigma_0)^n$. Here, n denotes the strain hardening exponent, σ_0 and ϵ_0 are the reference (yield) stress and strain, respectively. Guided by detailed numerical analyses employing a modified boundary layer (MBL) model, OS described the crack-tip fields in the form

$$\left(\sigma_{ij}\right)_{FB} = (\sigma_{ij})_{\mathrm{SSY}} + Q\sigma_0\delta_{ij} \tag{2}$$

where δ_{ij} denotes the Kronecker delta and the dimensionless second parameter Q defines the amount by which σ_{ij} in fracture specimens, $\left(\sigma_{yy}\right)_{FB}$, differ from the adopted high triaxiality reference SSY solution, $\left(\sigma_{yy}\right)_{\mathrm{SSY}}$. Consequently, Q is often defined as

$$Q \equiv \frac{\left(\sigma_{yy}\right)_{FB} - (\sigma_{yy})_{\mathrm{SSY}}}{\sigma_0} \tag{3}$$

where the difference field described is conventionally evaluated at the normalized crack-tip distance $r = 2J/\sigma_0$ which represents a microstructurally significant distance ahead of crack tip related to the operative fracture mechanism. OS and Cravero and Ruggieri [8] have also shown that Q is relatively independent of r in the range $1 \le r = 2J/\sigma_0 \le 5$. Construction of J-Q trajectories for structural components and fracture specimens then follows by evaluation of Eq. (3) at each stage of loading in the finite body. Figure 2(a) depicts the procedure to determine parameter Q for a moderate hardening material simply as the difference field at a given near-tip location; here, the computed difference between the SSY reference field and the finite body near-tip (opening) stress gradually increases with increasing remote loading as characterized by J. At similar values of the continuum, scalar parameters (J, Q), the crack-tip strain-stress fields which drive the local process have similar values as well.

Extension of the J-Q Approach for Growing Cracks

While the above framework was essentially developed for stationary cracks, the two-parameter description of near-tip stress states based on the Q constraint parameter can be extended to a steadily growing crack in a straightforward manner. Based upon the interpretation of Q as a measure of the level of stress triaxiality that quantifies the difference field relative to a high triaxiality reference stress state for a stationary crack, an alternative form applicable to growing cracks, denoted as Q^* in the present work, can be defined as

$$Q^* \equiv \frac{\left(\sigma_{yy}\right)_{FB}^{\Delta a} - (\sigma_{yy})_{\mathrm{SSY};\,\Delta a\,=\,0}}{\sigma_0} \tag{4}$$

where the difference field described is now evaluated at the *current* normalized crack-tip distance, $r^* = 2J/\sigma_0$ which represents the location of a material point ahead of the *advancing* crack tip.

Figure 2(b) shows the evolving near-tip (opening) stresses with increased amounts of ductile tearing, Δa, represented as a multiple of the cell size, D, for a moderate hardening material. Clearly, the tensile stress ahead of crack tip increases steadily with crack growth (compare the stress distributions for $\Delta a/D = 1$ and $\Delta a/D = 10$) thereby altering the corresponding levels of constraint (as measured by Q^*) with increased crack extension. These observations are entirely consistent with the previous investigation of Varias and Shih [23] and Dodds et al. [24] in which they have shown that crack growth under well-contained yielding elevates near-tip constraint. This issue is addressed in more details later in the article.

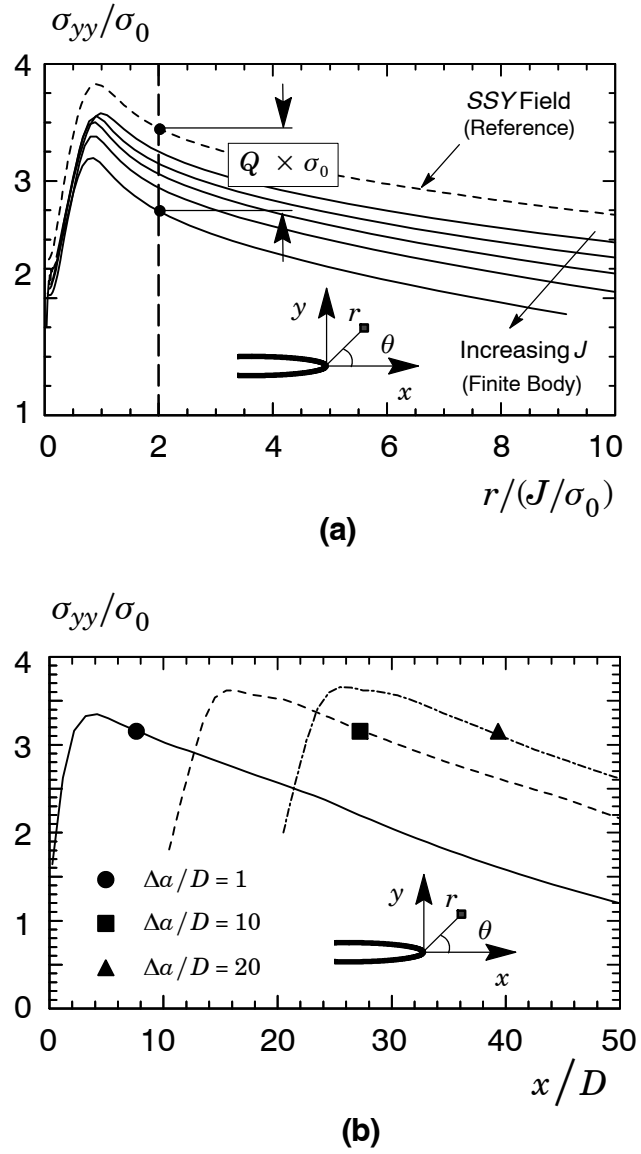

Figure 2. (a) *Procedure to determine parameter Q based on the difference field at a given near-tip location; (b) Schematic representation of the e*volving *near-tip (opening) stresses with increased amounts of ductile tearing*.

NUMERICAL PROCEDURES AND MATERIALS

Finite Element Models

Detailed finite element analyses are performed on plane-strain models for clamped SE(T) and 3P bend specimens having conventional 1-T geometry ($B = 25.4$ mm) with $W = 2B$ made of homogeneous material; these specimens are denoted as SE(T)$_C$ and SE(B). The analysis matrix includes specimens with $a/W = 0.2$, 0.3, 0.4, 0.5, $H/W = 10$ for the clamped SE(T) specimens and $S/W = 4$ for the SE(B) specimens. Here, a is the crack size, W is the specimen width, H defines the clamp distance and S represents the specimen span. Figure 3 shows the geometry and specimen dimensions for the analyzed crack configurations.

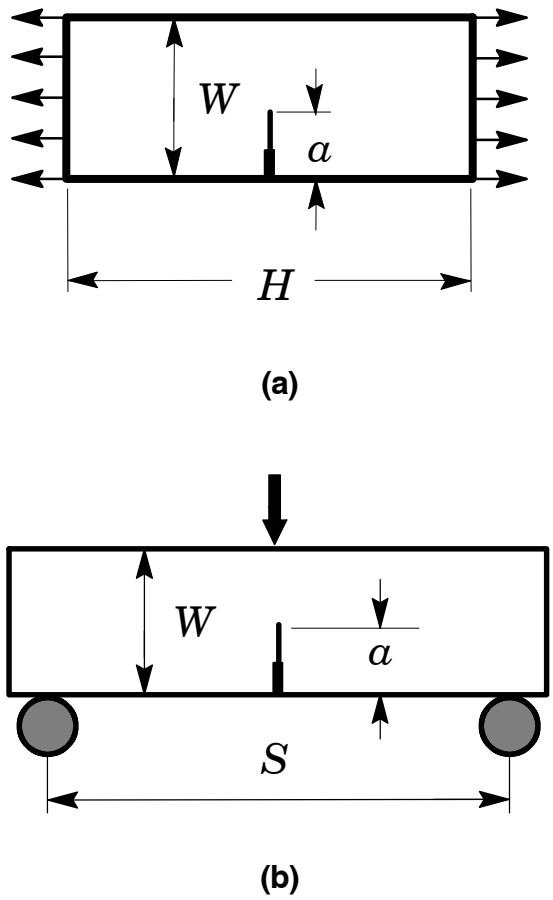

Figure 3. *Geometry for fracture specimens: a) SE(T) specimen with clamp conditions; b) 3P bend specimen.*

Figure 4 shows the finite element model constructed for the plane-strain analyses of the deeply-cracked SE(T) specimen with $a/W = 0.5$. All other crack models have very similar features. For stationary crack analyses, a conventional mesh configuration having a focused ring of elements surrounding the crack front is used with a small key-hole at the crack tip; the radius of the key-hole, ϱ_0, is 2.5μm (0.0025 mm). Symmetry conditions permit modeling of only one-half of the specimen with appropriate constraints imposed on the remaining ligament. A typical half-symmetric model has one thickness layer of 2717 8-node, 3-D

elements (2874 nodes) with plane-strain constraints imposed ($w = 0$) on each node. To achieve plane-strain conditions for the current study, a single thickness layer of the 3-D elements is defined with out-of-plane displacements constrained to vanish. The finite element models for the clamped and bend specimens are loaded by displacement increments imposed on the loading points. To simulate ductile crack extension in the fracture specimens, the finite element mesh for the growth analysis contains a row of ~ 120 computational cells along the remaining crack ligament ($W - a$) with fixed size of $D/2 \times D/2$ (see Fig. 1(b) and 4(c)). The initially blunted crack tip accommodates the intense plastic deformation and initiation of stable crack growth in the early part of ductile tearing.

Computational Procedures and Material Properties

The finite element code WARP3D [25] provides the numerical solutions for the plane-strain simulations reported here including stationary and crack growth analyses implementing the cell model. Evaluation of the J-integral derives from a domain integral procedure which yields J-values in excellent agreement with estimation schemes based upon η-factors for deformation plasticity [4] while, at the same time, retaining strong path independence for domains defined outside the highly strained material near the crack. WARP3D analyzes fracture models constructed with three-dimensional, 8-node tri-linear hexahedral elements. To achieve plane-strain conditions for the current study, a single

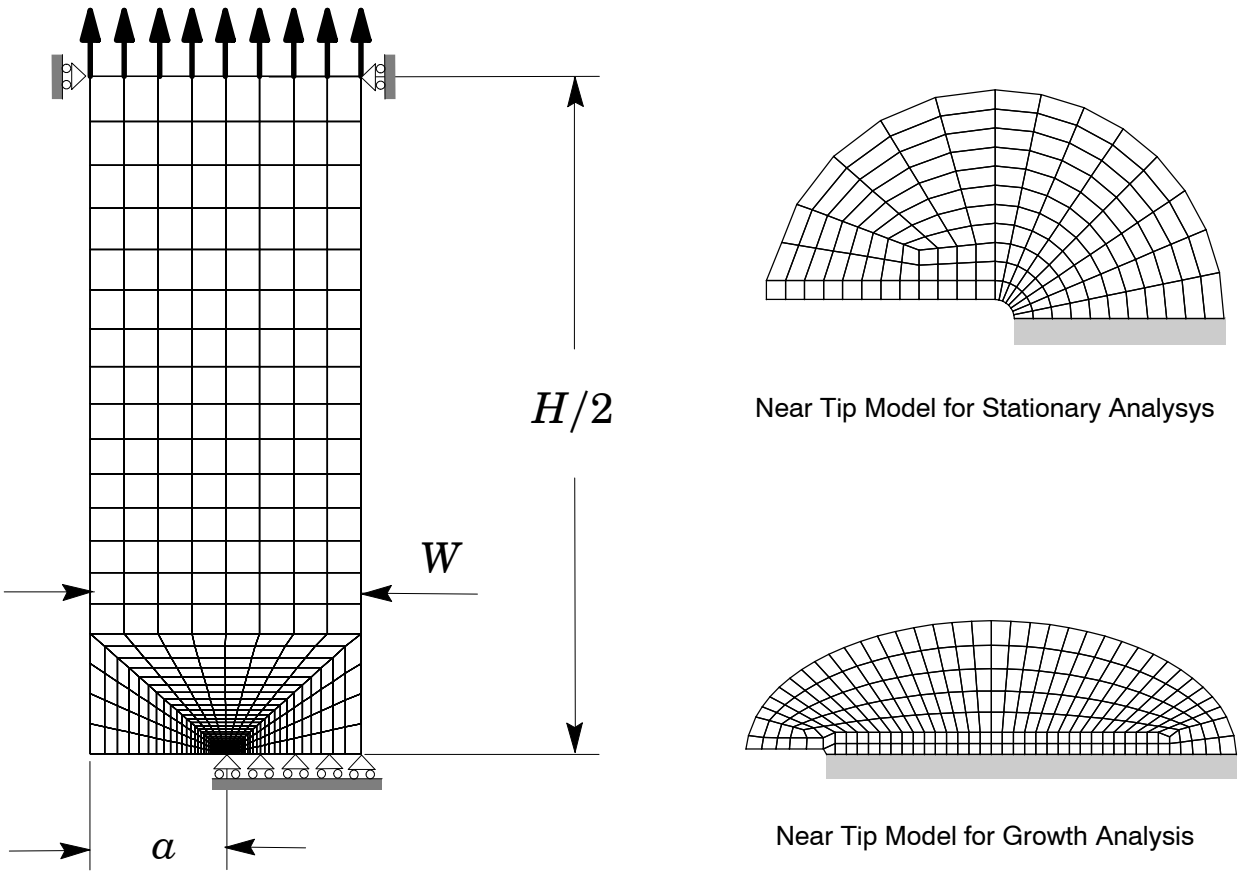

Figure 4. *Finite element model used in plane-strain analyses of the clamped SE(T) specimen with a/W = 0.5.*

thickness layer of the 3-D elements is defined with out-of-plane displacements constrained to vanish.

The elastic-plastic constitutive model employed in the stationary crack analyses utilizes a J_2 flow theory with conventional Mises plasticity in small geometry change (SGC) setting. The uniaxial true stress-logarithmic strain response for the material follows a piecewise linear approximation to the measured tensile response at room temperature described in Hippert and Ruggieri [26]. The material is an API 5L Grade X70 pipeline steel with 484 MPa yield stress (σ_{ys}) at room temperature (20°C) and relatively moderate-to-low hardening properties ($\sigma_{uts}/\sigma_{ys} \approx 1.22$), where σ_{uts} is the ultimate tensile strength. Figure 5 provides the engineering stress-strain curve for the tested pipeline steel (average of two tensile tests). Other mechanical properties include Young's modulus $E = 205$ GPa and Poisson's ratio $\nu = 0.3$. Hippert and Ruggieri [26] provide further details on the mechanical tensile test data and crack growth resistance testing using deeply cracked C(T) specimens for this material.

To describe the evolution of void growth and associated macroscopic material softening in the computational cells, the GT constitutive model given by Eq. (1) is adopted. The background material outside of the computational cells follows a J_2 flow theory in large geometry change (LGC) setting with the Mises plastic potential obtained by setting $f \equiv 0$ in Eq. (1). The uniaxial true stress-logarithmic strain response for both the background and cell matrix materials also follows a piecewise linear approximation to the measured tensile response for the API X70 pipeline steel described in [26] and shown in Fig. 5. Other mechanical properties for these analyses also include Young's modulus $E = 205$ GPa and Poisson's ratio $\nu = 0.3$.

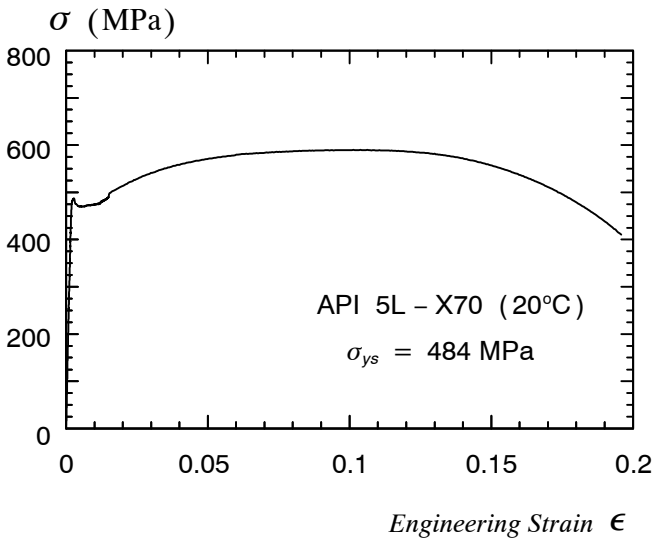

Figure 5. *Engineering stress-strain curve for the pipeline X70 steel employed in the analyses* [26].

Calibration of Cell Parameters

The cell model calibration scheme outlined previously has been applied to the pipeline steel employed in this study. The cell size D and initial porosity f_0 define the key parameters coupling the physical and computational models for ductile tearing. These parameters are calibrated using high constraint, deeply-cracked notch specimens to establish agreement between predicted and measured R-curves . The calibrated values for these parameters are then applied in similar analyses to predict the shallow notch R-curves. We note that other high constraint crack configurations, such as the deeply-cracked SE(B) specimen could be utilized to produce a specific set of cell parameters D and f_0. Here, the measured resistance curve for a deeply cracked C(T) specimen ($a/W = 0.65$) tested by Hippert and Ruggieri [26] is employed to calibrate these parameters.

Following their work, the cell size D employed in the numerical analyses is adopted as $D = 200$ μm.

Competing demands dictate the choice of cell size: (1) D must be representative of the large inclusion spacing to support arguments that it couples the physical and computational model, (2) predicted R-curves scale almost proportionally with D for fixed f_0 (a thicker layer requires more total work to reach critical conditions), (3) the mapping of one finite element per cell must provide adequate resolution of the stress-strain fields in the active layer and in the adjacent background material, (4) details of the continuum damage model, and (5) the type of finite element used (linear *vs*. quadratic). For the ferritic steels studied thus far with this model, calibrated cell sizes range from 50-200 μm with f_0 in the 0.0001-0.004 range. This range of values for D satisfies issue (1) while providing satisfactory resolution of the near-tip fields required in issue (3) after some tearing (calibrated values for D are comparable to the experimentally measured value for CTOD at initiation of ductile tearing). Very early in the loading history prior to ductile growth, these D values (with one-element-per-cell) may not provide sufficient resolution of the near-tip stress fields, for example, to quantify conditions for cleavage fracture. Moreover, because each change in D requires construction of a new mesh, it is obviously much less effort to fix D early on and then calibrate f_0. The calibrated values for D and f_0 clearly do not constitute a unique pair of parameters; for example, a slightly larger D value may be compensated for by a larger f_0 val-

ue. Nevertheless, there exists a reasonably narrow range of D and f_0 pairs which yield R-curves in agreement with the experimental results.

With parameter D fixed, the calibration process then focuses on determining a suitable value for the initial volume fraction, f_0, that produces the best fit to the measured crack growth data for the deeply cracked C(T) specimen. Figure 6 shows the measured and predicted J-Δa curves for this specimen. Predicted R-curves are shown for three values of the initial volume fraction, $f_0 = 0.0005$, 0.00075 and 0.001. For consistency, the location of the growing crack tip in the plane-strain analyses is taken at the cell with $f = 0.1$. This corresponds to a position between the cell currently undergoing extinction and the peak stress location; at this position stresses are decreasing rapidly and the void fraction is increasing sharply. Consequently, the use of slightly different f values, other than 0.1, to define the crack-tip location for plotting purposes does not appreciably alter the R-curves (at a fixed J, the amount of crack extension would vary only by a fraction of the cell size); Xia and Shih [10] and Ruggieri and Dodds [11] discuss this issue in detail. For $f_0 = 0.0005$, the predicted R-curve agrees well with the measured values for almost the entire range of growth, albeit lying a little above the measured data for $\Delta a \lesssim 1.0$ mm in the "blunting line" region. In contrast, the use of $f_0 = 0.001$ produces a lower resistance curve relative to the measured data. Consequently, the initial volume fraction $f_0 = 0.0005$ is thus taken as the calibrated (plane-strain) value for the API 5L-X70 steel used subsequently in this study.

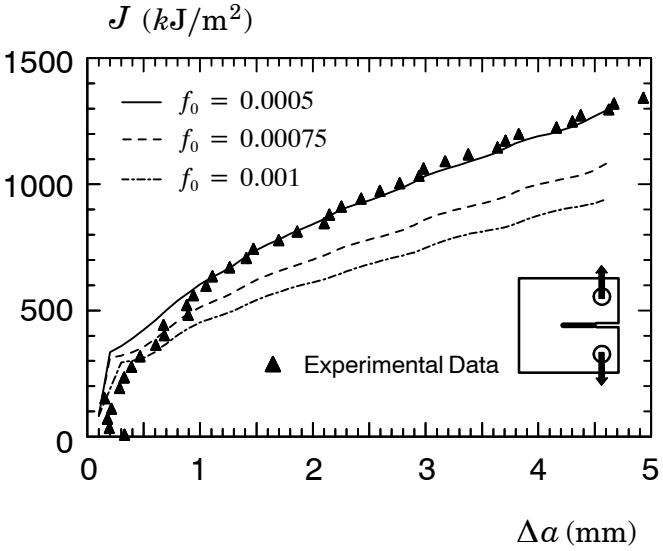

Figure 6. *Comparison of measured and predicted R-curve (plane-strain) for side-grooved 1(T) C(T) specimen of API 5L-X70 at room temperature [26].*

EVOLUTION OF CRACK-TIP CONSTRAINT IN SE(B) AND CLAMPED SE(T) FRACTURE SPECIMENS

J-Q Trajectories for Stationary Cracks

The extensive finite element analyses of SE(B) and SE(T) specimens for stationary cracks provide the basis to compare differences in constraint for these crack configurations in terms of the Q-solutions. Figure 7 displays the general effects of specimen geometry and loading mode on the J-Q trajectories for the analyzed fracture specimens. In all plots, Q is defined by Eq. (3) at the normalized distance ahead of crack tip given by $r = 2J/\sigma_0$ whereas J is normalized by $b_0\sigma_0$ with b_0 denoting the remaining initial crack ligament $W - a$ (notice that $J/b\sigma_0$ is plotted against $-Q$ to maintain positive scales). The material properties for all crack configurations were described previously and correspond to the tested API X70 pipeline steel. The research code FRACTUS2D [27] is employed to compute J-Q curves for each fracture specimen.

Consider first the evolution of Q with normalized J for the SE(B) specimen with varying a/W-ratio displayed in Fig. 7(a). Here, the Q-values depend markedly on crack size. For the deeply cracked SE(B) specimen with $a/W = 0.5$, the Q-parameter is positive at low load levels (note that the corresponding curve crosses the vertical axis of the plot at $J/b\sigma_0 \approx 0.01$) and gradually changes to negative values with increased levels of J. In contrast, the shallow crack SE(B) specimen reveals large negative Q-values almost immediately upon loading. Here, values for parameter Q ranging from -0.4 to -0.8 are associated with substantial reduction in the opening near-tip stresses for this specimen early in the loading.

Consider now the J-Q trajectories for the clamped SE(T) specimen with $H/W = 10$ and varying a/W-ratio shown in Fig. 7(b). A different picture now emerges as the corresponding Q-values become highly negative at relatively small load levels, particularly for the shallow cracked configurations ($a/W \approx 0.2 \sim 0.3$). An interesting development provided by these results is that all curves converge to a fixed Q-value of about 0.8. Further, note in Fig. 7(a) that the shallow cracked SE(B) specimen with $a/W = 0.2$ displays Q-values in the range -0.6 to -0.8 values, albeit displaying increased negative values with increased J-values, which is precisely the range of values for parameter Q in all analyzed clamped SE(T) specimens for

larger load levels ($J/b\sigma_0 \gtrsim 0.03$). Such behavior provides a particularly interesting result in that the shallow cracked SE(B) specimen and all analyzed SE(T) crack configurations have similar levels of constraint at larger values of J.

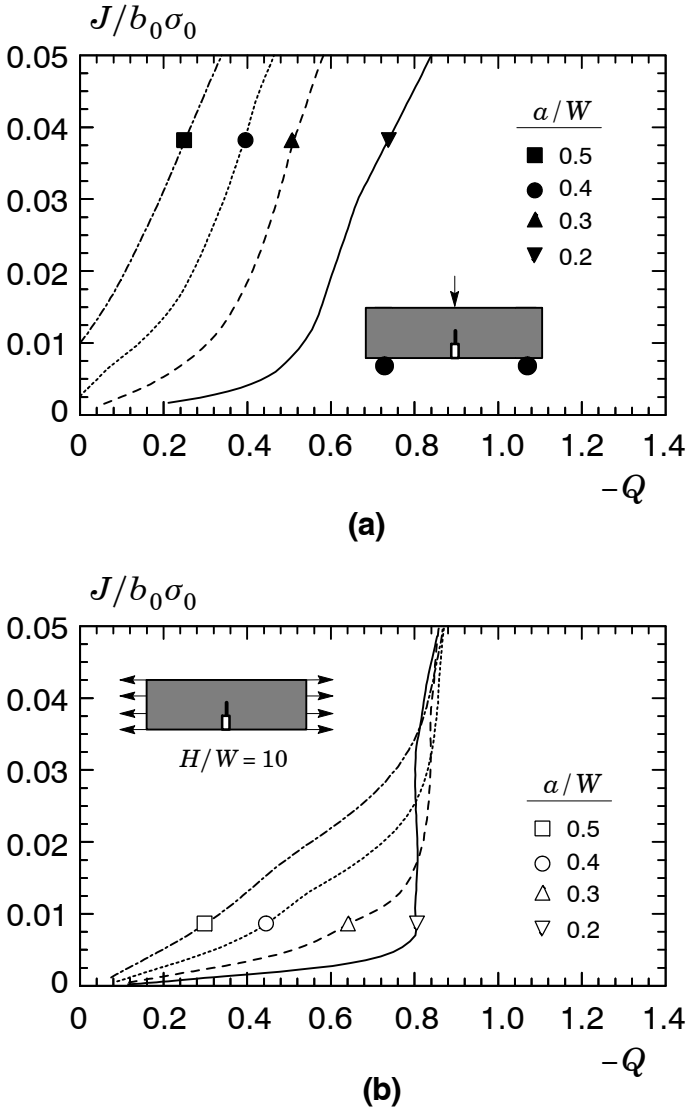

Figure 7. *Comparison of J-Q trajectories for 3P SE(B) and clamped SE(T) specimens with H/W = 10 for the API X70 steel and varying crack sizes.*

J-Q Trajectories for Growing Cracks

The J-Q trajectories for the SE(B) and SE(T) specimens based on a stationary crack analysis may not reflect changes in the near-tip stresses due to increased crack growth. In particular, since constraint loss with increased plastic deformation is potentially offset by the elevation in near-tip stresses due to steady growth of the crack, correlation of fracture behavior based on a stress triaxiality parameter defined for a stationary crack can be somewhat elusive. These features clearly justify addressing effects of crack growth on constraint variation for the fracture specimens considered here as reported below.

Figure 8(a) displays the computed crack growth resistance curves for the clamped SE(T) configuration with varying a/W-ratio. The analyses were conducted using the elastic-plastic properties for API X70 pipeline steel described earlier with the calibrated cell parameter, $f_0 = 0.0005$. The resistance curves are essentially the same in the "blunting line" region ($\Delta a \lesssim 0.2$ mm) and then rise steadily with increased J-values. It can be seen that the resistance curves depend rather weakly on the a/W-ratio. In particular, note that the fracture resistance behavior for the deeply cracked SE(T) specimens with $a/W = 0.4$ and 0.5 are almost indistinct from each other.

Figure 8(b) provides J-Q^* trajectories (which now incorporate effects of crack growth on the evolving near-tip stresses) for the clamped SE(T) specimens with different crack sizes. Similar to the previous analyses, here Q^* is defined by Eq. (4) at the normalized distance $r^* = 2J/\sigma_0$ whereas J is normalized by $b_0\sigma_0$ with b_0 denoting the remaining initial crack ligament $W-a$ (again $J/b_0\sigma_0$ is plotted against $-Q^*$ to maintain positive scales). The research code FRACTUS2D [27] is employed to compute J-Q^* curves for each fracture specimen. At early stages of loading ($J/b_0\sigma_0 \lesssim 0.02$), there is clearly an increase in crack-tip constraint relative to the stationary crack analysis as the Q^*-values vary from -0.8 to -0.4. Thereafter, all curves virtually merge into one single curve which shows that the constraint levels with increased crack growth for this specimen are almost independent of crack size (as measured by the a/W-ratio).

Attention is now directed to the effects of crack growth on fracture behavior for the SE(B) specimen. Figure 9(a) shows the computed crack growth resistance curves for the shallow ($a/W = 0.2$) and deeply-cracked ($a/W = 0.5$) SE(B) configuration. Figure 9(b) displays J-Q^* trajectories for these SE(B) specimens including effects of crack growth. The significant features include: (1) effects of crack size (a/W-ratio) on the resistance curves are more prominent for this specimen geometry; (2) there is also no effect in the "blunting line" region of the resistance curves for both the shallow and deeply cracked configurations and 3) after an increase in crack-tip constraint at early stages of loading, the rising J-Q^* trajectories for both specimen geometries differ significantly; here the Q^*-values for the SE(B) speci-

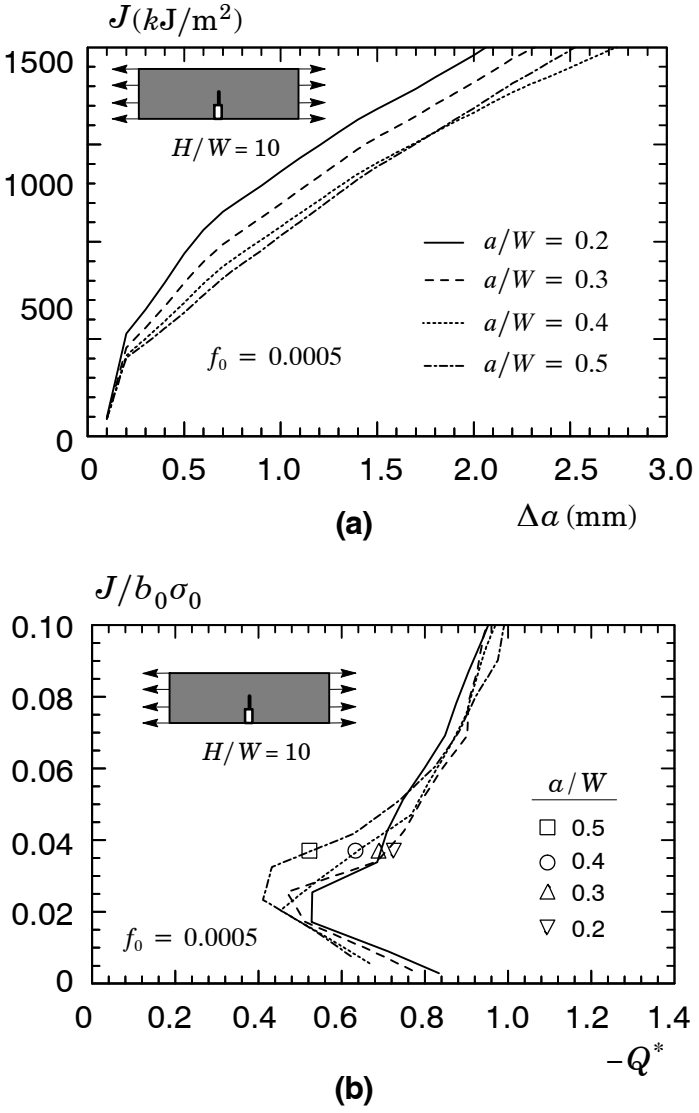

Figure 8. *Computed fracture behavior for clamped SE(T) specimens with H/W = 10 for the API X70 steel and varying crack sizes: (a) crack growth resistance curves; (b) J-Q* trajectories*

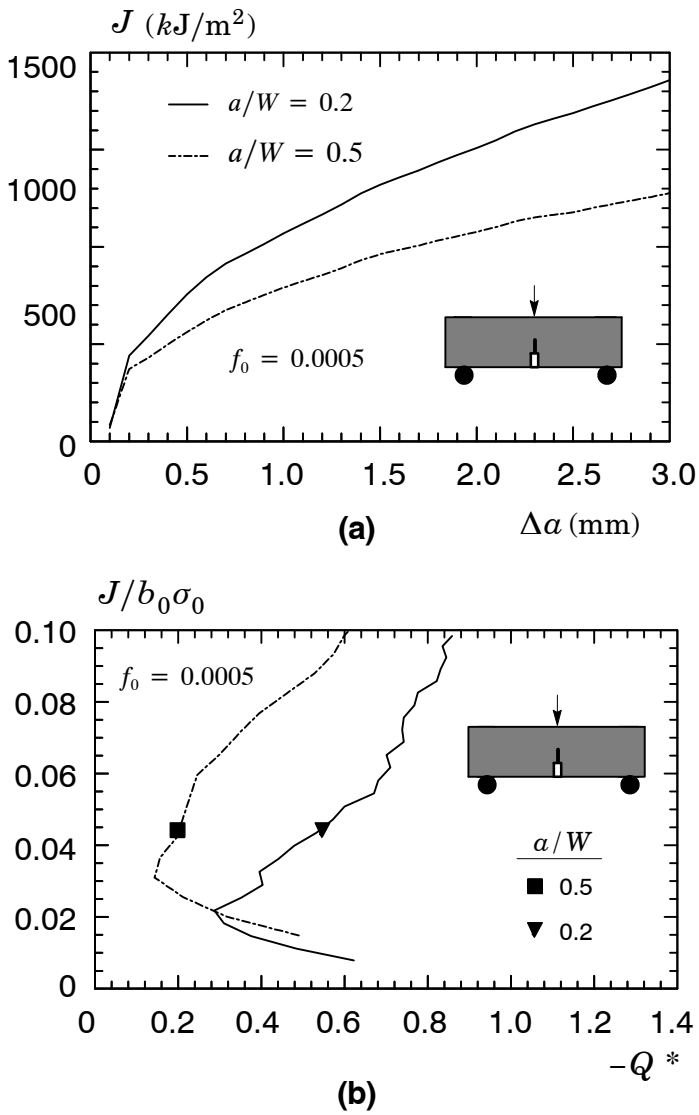

Figure 9. *Computed fracture behavior for SE(B) specimens for the API X70 steel and varying crack sizes: (a) crack growth resistance curves; (b) J-Q* trajectories*

men with $a/W = 0.2$ vary from -0.3 to -0.8 over almost the entire range of loading (characterized by J) considered. This last feature provides a particularly interesting result in that the constraint levels with increased crack growth for the shallow cracked SE(B) specimen compare well with the corresponding constraint levels for the clamped SE(T) specimens displayed in previous Fig. 8(b).

DISCUSSION AND CONCLUDING REMARKS

This brief study addresses an extension of the *J-Q* approach, supplemented by a micromechanics approach to model ductile tearing using computational cells, to describe constraint effects on ductile crack growth in SE(B) and SE(T) fracture specimens. The methodology enables evaluation of *J-Q* trajectories (and associated measures of crack-tip constraint) which incorporate changes

in th evolving near-tip stresses due to steady crack growth that would otherwise be neglected in conventional, stationary crack analyses. The framework thus provides further insight and additional understanding in the correlation of fracture behavior for fracture specimens (and possibly to cracked structural components as well) based on a stress triaxiality parameter.

In using the results presented in this article to discuss a proper characterization of ductile fracture behavior depending on specimen geometry, it is well to keep in mind the difficulties in comparing (and accurately defining) constraint levels for stationary and growing cracks. Varias and Shih [23] and Dodds et al [24] address this issue in detail. In particular, Dodds et al [24] points out the complex interacting effects of specimen geometry, crack size, tearing modulus and strain hardening behavior on the evolving near-tip stress states which drive the ductile fracture process.

To illustrate this point, it is instructive to make use of the fracture resistance test data obtained by Mathias et al. [28] for a girth weld made of an API 5L X80 pipeline steel using shallow crack SE(B) specimens and deeply-cracked SE(T) specimens with clamp conditions. Annex A provides a brief overview of the fracture testing details and crack growth resistance curves (J-Δa) at room temperature derived from the unloading compliance procedure. The shallow-crack SE(B) specimen provides a resistance curve which, albeit slightly more conservative, exhibits levels of J-values comparable to the levels of J corresponding to the deeply-cracked SE(T) specimen at a fixed amount of crack growth, Δa. However, differences between the J-Δa curves for the tested crack configurations are perhaps somewhat larger than would be expected from the analyses conducted previously but which can be nevertheless considered acceptable given the advantages of testing smaller specimens. Additional work is in progress to further validate the use of shallow-crack SE(B) specimens as an alternative fracture specimen to measure crack growth properties for pipeline steels and girth welds. Ongoing investigation also focuses on establishing robust correlations between J and CTOD for stationary and growing cracks in SE(T) and SE(B) fracture specimens.

Acknowledgments

This investigation is supported by the Brazilian Scientific Council for Research and Technology (CNPq) (Grant 304132/2009-8) and by Fundação de Amparo à Pesquisa do Estado de São Paulo (FAPESP Grant 2009/54229-3).

References

[1] American Society for Testing and Materials, “Standard Test Method for Measurement of Fracture Toughness”, ASTM E1820, 2011.

[2] International Standard Organization, “Metallic Materials - Method of Test for the Determination of Quasistatic Fracture Toughness of Welds”, ISO 15653, 2010.

[3] Hutchinson, J. W., ‘‘Fundamentals of the Phenomenological Theory of Nonlinear Fracture Mechanics,’’ *Journal of Applied Mechanics*, Vol. 50, pp. 1042-1051, 1983.

[4] Anderson, T. L. *Fracture Mechanics: Fundaments and Applications - 3rd Edition*, CRC Press, New York, 2005.

[5] Eiber, R. J. and Kiefner, J. F. “Failure of Pipelines”, in Metals Handbook, Ninth Edition, Vol. 11 - Failure Analysis and Prevention, American Society for Metals, pp. 695-706, 1986.

[6] Nyhus, B., Polanco, M and Ørjasæter, O., ‘‘SENT Specimens as an Alternative to SENB Specimens for Fracture Mechanics Testing of Pipelines.” *in* ASME International Conference on Offshore Mechanics and Arctic Engineering (OMAE 2003), American Society of Mechanical Engineers, Cancun, Mexico, 2003.

[7] Det Norske Veritas, “Fracture Control for Pipeline Installation Methods Introducing Cyclic Plastic Strain”, Recommended Practice DNV-RP-F108, 2006.

[8] Cravero, S. and Ruggieri, C., “Correlation of Fracture Behavior in High Pressure Pipelines with Axial Flaws Using Constraint Designed Test Specimens - Part I: Plane-Strain Analyses,” *Engineering Fracture Mechanics*, Vol. 72, pp. 1344-1360, 2005.

[9] Park, D. Y., Tyson, W. R., Gianetto, J. A., Shen, G and Eagleson, R. S., “Evaluation of FRacture Toughness of X100 Pipe Steel Using SE(B) and Clamped SE(T) Single Specimens,” *in* ASME International Pipeline Conference (IPC 2010), American Society of Mechanical Engineers, Calgary, Canada, 2010.

[10] Xia, L. and Shih, C.F., “Ductile Crack Growth – I. A numerical study using computational cells with microstructurally–based length scales”, Journal of the Mechanics and Physics of Solids, vol.43, pp.233–259, 1995.

[11] Ruggieri, C. and Dodds, R. H., ‘‘Numerical Modeling of Ductile Crack Growth in 3-D Using Computational Cell Elements,” *International Journal of Fracture*, Vol. 82, pp. 67-95, 1996.

[12] Gullerud, A. S., Gao, X., Dodds, R. H. and Haj-Ali, R. “Simulation of Ductile Crack Growth Using Computational Cells: Numerical Aspects.” *Engineering Fracture Mechanics*, Vol. 66, pp. 65-92, 2000.

[13] Garrison, W. M. Jr. and Moody, N. R., “Ductile fracture”, Journal of the Physics and Chemistry of Solids, vol. 48, pp.1035-1074, 1987.

[14] Gurson , A.L., ”Continuum Theory of Ductile Rupture by void nucleation and growth: Part I – Yield Criteria and Flow rules for porous ductile media”. Journal of Engineering Materials and Technology, vol.99, pp. 2–15, 1977.

[15] Tvergaard, V., ”Material Failure by void growth to coalescence”. Advances in Applied Mechanics, vol. 27, pp83–151, 1990.

[16] Faleskog, J., and Shih, C.F., “Cell Model for Nonlinear Fracture Analysis - I: Micromechanics Calibration,” *International Journal of Fracture*, Vol. 89, pp. 355-373, 1998.

[17] Nevalnien, M. and Dodds, R. H. ''Numerical Investigation of 3−D Constraint Effects on Brittle Fracture in SE(B) and C(T) Specimens," *International Journal of Fracture*, Vol 74, pp. 131-161, 1995.

[18] Dodds, R. H., Shih, C. F., and Anderson, T. L. ''Continuum and Micro-Mechanics Treatment of Constraint in Fracture," *International Journal of Fracture*, Vol. 64, pp. 101-133, 1993.

[19] Joyce, J. A., Hackett, E. M. and Roe, C., "Effects of Crack Depth and Mode Loading on the *J-R* Curve Behavior of a High Strength Steel," *Constraint Effects in Fracture, ASTM STP 1171*, E. M. Hackett, et al. Eds., American Society for Testing and Materials, Philadelphia, pp. 239-263, 1993.

[20] Joyce, J. A., and Link R. E., "Effects of Constraint on Upper Shelf Fracture Toughness," *Fracture Mechanics, 26th Volume, ASTM STP 1256*, W. G. Reuter, et al. Eds., American Society for Testing and Materials, Philadelphia, pp. 142-177, 1995.

[21] O'Dowd, N. P., and Shih, C. F., ''Family of Crack-Tip Fields Characterized by a Triaxiality Parameter: Part I - Structure of Fields,'' *Journal of the Mechanics and Physics of Solids*, Vol. 39., No. 8, pp. 989-1015, 1991.

[22] O'Dowd, N. P., and Shih, C. F., ''Family of Crack-Tip Fields Characterized by a Triaxiality Parameter: Part II - Fracture Applications,'' *Journal of the Mechanics and Physics of Solids*, Vol. 40, pp. 939-963, 1992.

[23] Varias A.G. and Shih C. F., "Quasi-Static Crack Advance Under a Range of Constraint Steady-State Fields Based on a Characteristic Length," *Journal of the Mechanics and Physics of Solids*, Vol. 41., No. 5, pp. 835-861, 1993.

[24] Dodds, R. H., Tang, M. and Andareson, T., "Numerical Modeling of Ductile tearing on Cleavage Fracture Toughness," *Constraint Effects in Fracture: Theory and Application, ASTM STP 1244*, M. Kirk and A. Bakker, Eds., American Society for Testing and Materials, Philadelphia, pp. 100-133, 1995.

[25] Gullerud, A., Koppenhoefer, K., Roy, A., RoyChowdhury, S., Walters, M., Bichon, B., Cochran, K. and Dodds, R., ''WARP3D: Dynamic Nonlinear Fracture Analysis of Solids Using a Parallel Computers and Workstations".'' *Structural Research Series (SRS) 607*. UILU-ENG-95-2012. University of Illinois at Urbana-Champaign. 2004.

[26] Hippert, E. and Ruggieri, C., "Experimental and Numerical Investigation of Ductile Crack Extension in a High Strength Pipeline Steel," *in* ASME Pressure Vessel and Piping Conference (PVP 2001), American Society of Mechanical Engineers, Atlanta, GA, 2001.

[27] Ruggieri, C., "FRACTUS2D: Numerical Computation of Fracture Mechanics Parameters for 2-D Cracked Solids," EPUSP, University of São Paulo, 2011.

[28] Mathias, L. L. S., Sarzosa, D. F. B. and Ruggieri, C., "Effects of Specimen Geometry and Loading Mode on Crack Growth Resistance Curves of a High-Strength Pipeline Girth Welds". *International Journal of Pressure Vessels and Piping* (Submitted for Publication).

APPENDIX

Mathias et al. [28] reported on a series of fracture tests conducted on weld specimens made of a pipeline steel. The tested weld joint was made from an API X80 UOE pipe having thickness, $t_w = 19$ mm. Girth welding of the pipe was performed using the FCAW process in the 1G (flat) position with a single V-groove configuration in which the root pass was made by GMAW welding.

Unloading compliance (UC) tests at room temperature were performed on center notch weld, clamped SE(T) specimens with a fixed overall geometry and crack length to width ratios, a/W, to measure tearing resistance curves in terms of J-Δa. The clamped SE(T) specimens have $a/W = 0.4$ and $H/W = 10$ with thickness $B = 14.8$ mm, width $W = 14.8$ mm and clamp distance $H = 148$ mm (refer to Fig. 10(a)). Here, a is the crack depth and W is the specimen width which is slightly smaller that the pipe thickness, t_w. UC tests at room temperature were also conducted on center notched welded SE(B) specimens with $a/W = 0.25$ with thickness $B = 14.8$ mm, width $W = 14.8$ mm and span $S = 4W$ (refer to Fig. 10(b)). Conducted as part of a collaborative program, testing of these specimens focused on the development of accurate procedures to evaluate crack growth resistance data for pipeline girth welds.

All specimens, including the SE(T) configuration, were precracked in bending using a three-point bend apparatus. After fatigue precracking, the specimens were side-grooved to a net thickness of $\sim 85\%$ the overall thickness (7.5% side-groove on each side) to promote uniform crack growth and tested following some general guidelines described in ASTM E1820 standard [1]. Records of load *vs.* crack mouth opening displacements (CMOD) were obtained for the specimens using a clip gauge mounted on knife edges attached to the specimen surface. Figure 11 shows the measured load-displacement curve (as described by CMOD) for both test specimens.

Evaluation of the crack growth resistance curve follows from determining J and Δa at each unloading point of the measured load-displacement data. Mathias et al. [28] provide further details of the procedure to determine J and Δa based upon η-factors and compliance functions previously derived by Ruggieri [27]. Figure 12 presents the measured crack growth resistance curves for the tested pipelines girth weld using clamped SE(T) and 3P SE(B) specimens. The shallow-crack SE(B) specimen exhibits a resistance curve which, albeit slightly more conservative, exhibits levels of J-values comparable to the levels of J corresponding to the deeply-cracked SE(T) specimen at a fixed amount of crack growth, Δa.

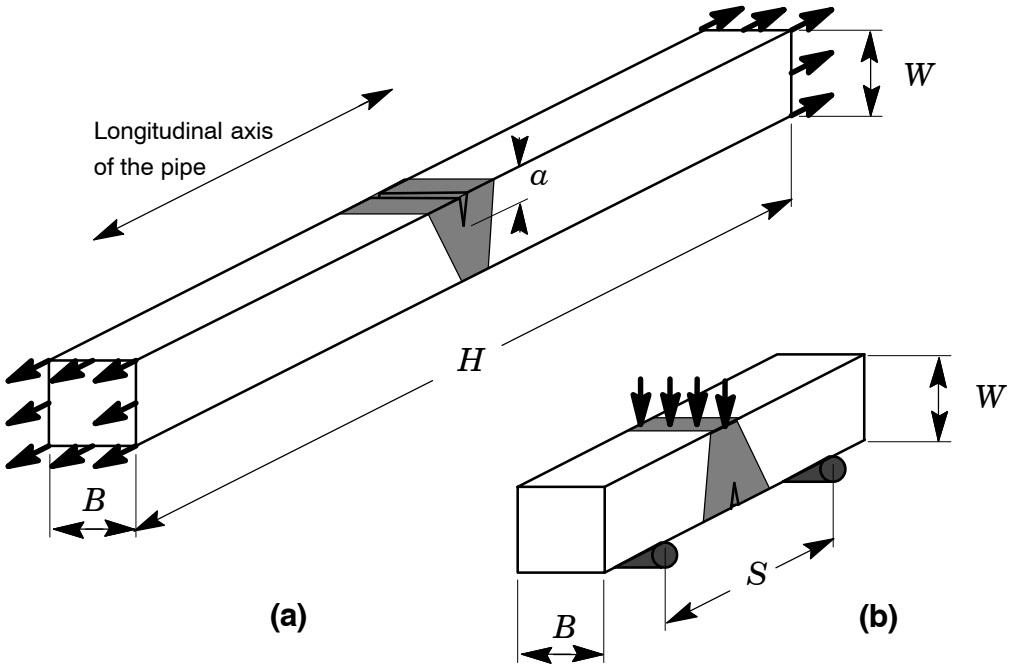

Figure 10. *Geometry of tested fracture specimens with weld centerline notch. (a) Clamped SE(T) specimen with a/W = 0.4 and H/W = 10; (b) 3P SE(B) specimens with a/W = 0.25 and S/W = 4 (BxB configuration).*

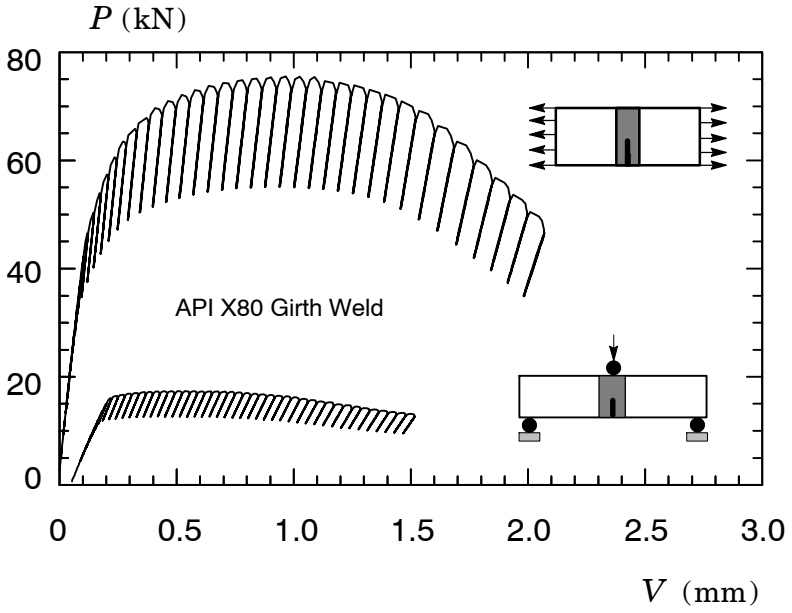

Figure 11. *Measured load-CMOD curve for the tested X80 pipeline girth weld using clamped SE(T) specimens with a/W = 0.4 and 3P SE(B) specimens with a/W = 0.25 [28].*

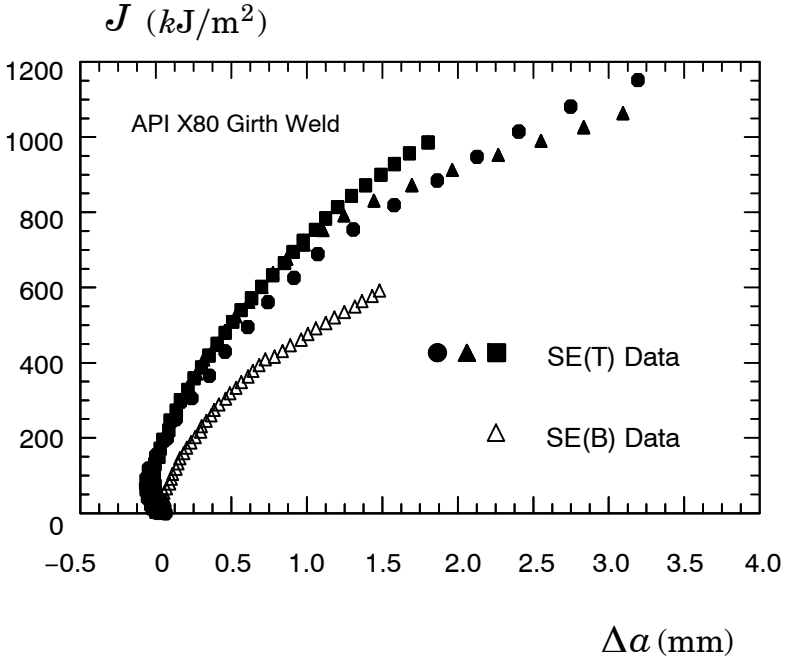

Figure 12. *Experimental R−curves for tested clamped SE(T) and 3P SE(B) specimens based upon the UC procedure [28]*